Composite Structures 118 (2014) 403–415

Contents lists available at ScienceDirect

Composite Structures

journal homepage: www.elsevier.com/locate/compstruct

Reducing the seismic damage of reinforced concrete frames using FRP confinement

Vui Van Cao, Hamid Reza Ronagh *

School of Civil Engineering, The University of Queensland, St. Lucia, Australia

ARTICLE INFO

Article history:
Available online 4 August 2014

Keywords:
FRP
Confinement
Damage assessment
RC frame
Seismic load

ABSTRACT

The objective of this study is to investigate the effect of FRP confinement on reducing the damage of an 8-storey poorly-confined reinforced concrete frame subjected to different seismic intensities. Inelastic time history and damage analyses are performed for the poorly-confined frame and its FRP retrofit. Analyses are also performed for a geometrically similar frame designed with the more restrictive requirements of an intermediate frame for comparison with the poorly-confined and retrofitted frames. The results confirm the positive effect of FRP confinement significantly reducing the damage of the poorly-confined frame down one or two damage levels. The comparison reveals that the poorly-confined frame has been essentially upgraded to the intermediate frame. The results are useful for structural designers working in retrofitting area. The limitation of this study is also presented.

1. Introduction

Important roles of transverse reinforcement in reinforced concrete (RC) structures are (1) to prevent buckling of longitudinal bars; (2) to prevent shear failure and (3) to confine the concrete [1]. A large number of buildings in different parts of the world are identified deficient with respect to their transverse reinforcement when measured against the requirements of modern codes. Many of these had been designed and built based on older codes, in which the earthquake loads were given a lower emphasis comparing to today's practice while gravity loads were considered as the major design loads. Consequently, these structures are not ductile enough to absorb the seismic energy demand and thus are vulnerable to earthquakes as has become evident in the past recent earthquake events such as Northridge (1994), Kobe (1995), Chi-Chi (1999), Bam (2003), Christchurch (2011). Mitigating the seismic hazards for these deficient structures, instead of replacing, has been increasingly looked at by the engineering community due to economic reasons.

Fortunately, the availability of advanced building materials such as Fibre Reinforced Polymer (FRP) at lower costs provides economical solutions to upgrade these deficient buildings. FRP with its distinct characteristics such as high strength, lightweight and ease of application has been increasingly becoming the material of choice. Numerous studies have been undertaken to evaluate the effects of FRP in upgrading deficient RC structures.

FRP can be used to increase confinement, a favourable situation for concrete. A great enhancement in the stress–strain behaviour of concrete confined by FRP can be achieved. This has been understood and proven in the past and a number of models for this behaviour, which are later discussed in details in Section 2.2, have been proposed by researchers [2–5]. FRP confinement greatly enhances the performance of columns benefitting from the enhanced properties of concrete under confinement. Harajli and Rteil [6] experimentally investigated the confinement effect of FRP and compared with that of steel stirrups on rectangular RC columns. Their results indicated that energy absorption and dissipation capability of the FRP confined columns was superior in comparison with that of the columns confined by steel stirrups. Sheikh and Yau [7] performed an experiment on 6 circular columns retrofitted by FRP jacket subjected to lateral cyclic displacements with a constant axial load and showed enhancement of strength, ductility and energy absorption of these retrofitted columns. Recently, Rahai and Akbarpour [8] conducted experimental and analytical studies on FRP confined rectangular RC columns subjected to axial and bending loads. Their results indicated a significant improvement of the strength and ductility of these confined columns. The FRP confinement, in combination with FRP flexural strengthening, was also investigated by Mukherjee and Joshi [9] in their experimental study on FRP retrofitted beam-column joints. They concluded that there were a considerable improvement of yield load, initial stiffness and energy dissipation capacity.

* Corresponding author.
E-mail address: h.ronagh@uq.edu.au (H.R. Ronagh).

http://dx.doi.org/10.1016/j.compstruct.2014.07.038
0263-8223/

At the macro level, Balsamo et al. [10] conducted a study on a 4-storey RC frame with columns and beams wrapped by FRP. They concluded that the FRP retrofitted frame can withstand 1.5 times the intensity of the design earthquake. A few years later, Ludovico et al. [11,12] performed experimental and analytical studies on gravity-load designed and retrofitted full scale three-storey RC structures subjected to seismic intensities of 0.2 g and 0.3 g. FRP confinement was applied to the columns while shear and flexural strengthening were applied to the beams. The Balsamo et al.'s [10] conclusion was reaffirmed [11,12]. They also concluded that the deformation capacity of the retrofitted structure increased considerably and less damage of the retrofitted structure was observed in the experiments [12]. A similar study of retrofitting combining confinement and flexure was carried out by Garcia et al. [13] for the original and FRP retrofitted damaged full scale 2-storey RC frames subjected to different shaking levels. They confirmed that the performance of the retrofitted frame was substantially improved; desirable beam-sway mechanism was achieved and the deformability capacity of the columns increased significantly. In the same year, Mortezaei et al. [14] conducted a study on FRP retrofitted of different RC frames subjected to near-fault ground motions with fling step. The FRP confinement of columns and flexural effect on beams were proved to result in increases of 1.5 times and 2.3 times the shear capacity and the energy dissipation of the retrofitted frame, respectively. Eslami and Ronagh [15] used FRP to confine columns at the critical zones of an 8-storey poorly-confined frame. Their analytical results showed that the seismic performance and ductility increased substantially.

FRP confinement demonstrates the above favourable effects; however, studies on the effects it can have on reducing the potential damage of multistorey RC frames subjected to seismic loads are seldom found in literature. The objective of this study is to explore the effect of FRP confinement in terms of reduction of potential damage expressed by a damage index. An 8-storey poorly-confined (due to deficiency of transverse reinforcement) RC structure is chosen for this purpose. A geometrically similar structure but with seismically adequate transverse reinforcement according to "intermediate" detailing requirements is designed. The poorly-confined, the intermediate and the FRP retrofitted frames are modelled in SAP2000 [16] using nonlinear LINK elements. Inelastic time history analyses are conducted for different seismic intensities regulated in current seismic codes. The damage of poorly-confined and retrofitted frames is compared with one another and with that of the intermediate frame. The results show the favourable effect of FRP confinement on reducing the potential damage. The comparison reveals that the poorly-confined frame has been upgraded to the intermediate frame. For the numerical model to work properly, correct modelling of the material property is needed. This is explained below followed by the numerical model and the results.

2. Behaviour of concrete confined by transverse reinforcement and FRP

2.1. Behaviour of concrete confined by transverse reinforcement

The stress–strain behaviour of concrete confined by rectangular stirrups has been extensively studied by researchers and different models have been proposed [17–21]. The features of these models were combined in the model proposed by Kent and Park [22], in which the stress–strain relationship up to maximum stress is the same as that of unconfined model and the strain at the maximum stress remains unchanged at 0.002. The difference between confined and unconfined concrete is the descending branch after the maximum stress. Therefore, the Kent and Park [22] model is conservative in most cases as it does not take into account the increase in the maximum stress of confined concrete [23]. In recognition of this issue, Park et al. [24] modified the original Kent and Park [22] model taking into account the enhancement of concrete strength due to confinement. This modified model is selected for use in this paper. It is described by Eqs. (1), (2), followed by Eqs. (3)–(6).

$$f_c = f_c''\left[\frac{2\varepsilon_c}{\varepsilon_o} - \left(\frac{2\varepsilon_c}{\varepsilon_o}\right)^2\right] \text{ if } \varepsilon_c \leqslant \varepsilon_o \tag{1}$$

$$f_c = f_c''[1 - Z(\varepsilon_c - \varepsilon_o)] \geqslant 0.2f_c'' \text{ if } \varepsilon_c \leqslant \varepsilon_o \tag{2}$$

in which

$$f_c'' = Kf_c' \tag{3}$$

$$\varepsilon_o = 0.002K \tag{4}$$

$$Z = \frac{0.5}{\frac{3+0.29f_c'}{145f_c'-1000} + \frac{3}{4}\rho_s\sqrt{\frac{b''}{s_h}} - 0.002K} \tag{5}$$

$$K = 1 + \frac{\rho_s f_{yh}}{f_c'} \tag{6}$$

where, f_c is stress, ε_c is the strain of concrete, ρ_s is the ratio of the volume of rectangular steel hoops to the volume of concrete core measured to the outside of the peripheral hoop, f_c' is the maximum stress in MPa, b'' is the width of the concrete core measured to outside of the peripheral hoop, s_h is the centre-to-centre spacing of hoop sets.

2.2. Behaviour of concrete confined by FRP

FRP can make the concrete confined, resulting in a significant increase of the strength and ductility of concrete. This has been proved by numerous researchers [2,3,25–28]. Their stress–strain models of FRP confined concrete can be divided into two categories: with and without internal transverse reinforcement. For the case with internal transverse reinforcement, it would be appropriate if two separate models are simultaneously considered: one model is applied for the concrete core surrounded by transverse reinforcement, which is confined both internally by stirrups and externally by FRP; another model is applied for the outer part of the concrete (the cover) which is confined only by FRP. However, this seems to be complicated due to the interaction of these internal and external confinements.

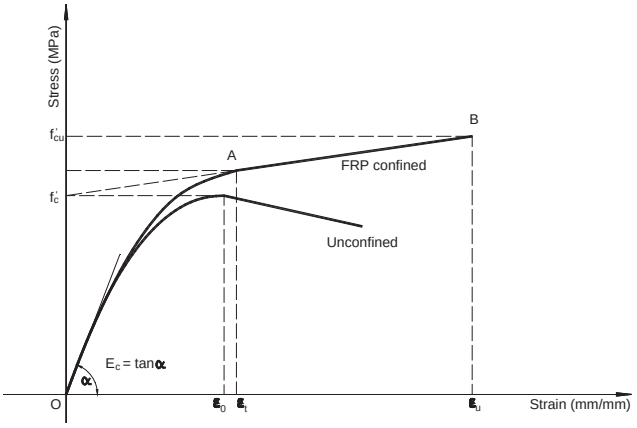

Fig. 1. Lam and Teng [2,25] model for FRP confined concrete.

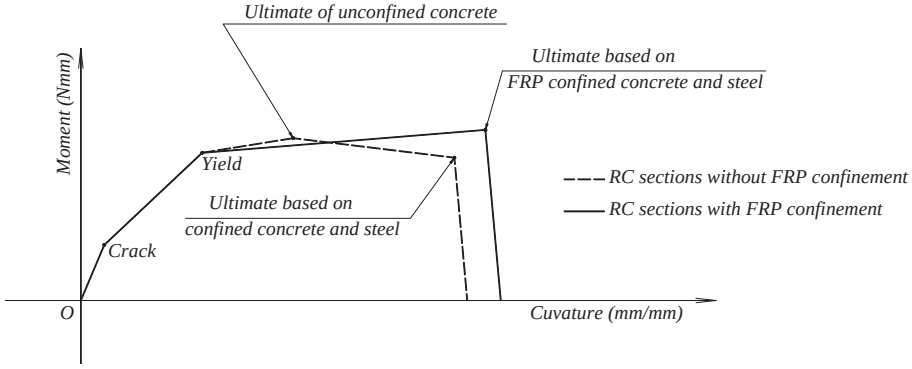

Fig. 2. Moment–curvature curves of RC sections with and without FRP confinement.

Additionally, the confinement due to FRP is much stronger than that due to transverse reinforcement. This is expected as the stress of concrete with a proper FRP confinement increases after the strain of around 0.002 (Fig. 1); however, after this strain, there is a descending branch in the stress–strain curve of concrete confined by stirrups as shown in Eq. (2). Furthermore, FRP is often chosen to provide confinement for poorly-confined RC members. Thus, the poor confinement of deficient stirrups can be neglected when the FRP becomes effective.

For simplification, together with the above reasons, models without internal transverse reinforcement are considered for use. Amongst the available models, Lam and Teng [2,25] model, which was proven to be most suitable for circular and rectangular columns [29], and has been used in a number of studies [15,29], is selected in the current study. Fig. 1 shows the Lam and Teng [2,25] model, in which, the stress–strain relationship of concrete confined by FRP is described by two regions expressed by Eqs. (7) and (8), followed by Eqs. (9)–(18).

$$\text{Region OA } (0 \leqslant \varepsilon_c \leqslant \varepsilon_t): \; f_c = E_c\varepsilon_c - \frac{(E_c - E_2)^2}{4f'_c}\varepsilon_c^2 \tag{7}$$

$$\text{Region AB } (\varepsilon_t \leqslant \varepsilon_c \leqslant \varepsilon_u): f_c = f'_c + E_2\varepsilon_c \tag{8}$$

$$\text{where, } \varepsilon_t = \frac{2f'_c}{E_c - E_2} \tag{9}$$

$$E_2 = \frac{f'_{cu} - f'_c}{\varepsilon_u} \tag{10}$$

in which, f'_{cu} and ε_u are the axial stress and corresponding axial strain at ultimate.

For the general case of rectangular columns, the ultimate strength f'_{cu} and strain ε_u are expressed taking into account the reduced efficiency of rectangular sections as follows

$$f'_{cu} = f'_c\left[1 + 3.3k_{s1}\frac{f_{la}}{f'_c}\right] \text{ if } \frac{f_{la}}{f'_c} \geqslant 0.07 \tag{11}$$

$$f'_{cu} = f'_c \text{ if } \frac{f_{la}}{f'_c} < 0.07 \tag{12}$$

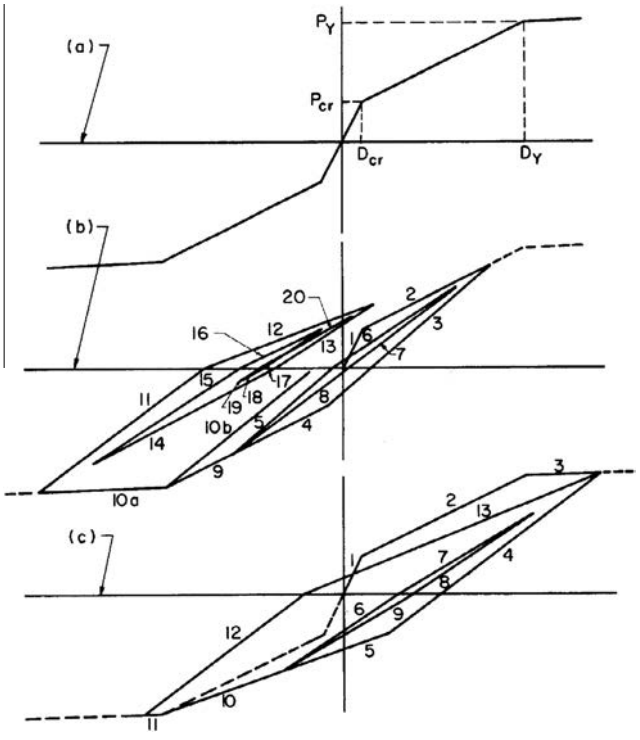

Fig. 3. Load–deflection relationship [33].

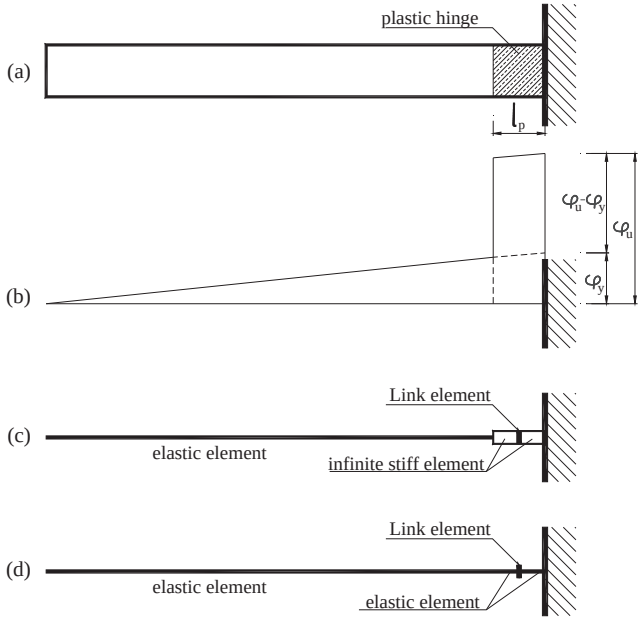

Fig. 4. Theoretical background of modelling with nonlinear LINK element.

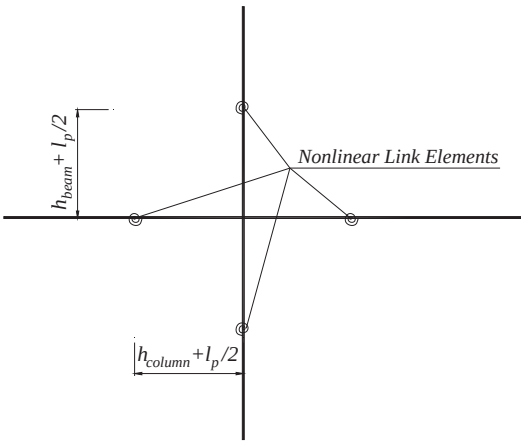

Fig. 5. Nonlinear LINK locations of beams and columns in frames.

$$\varepsilon_u = \varepsilon_o \left[1.75 + 12 k_{s2} \frac{f_{la}}{f'_c} \left(\frac{\varepsilon_{h,rup}}{\varepsilon_o} \right)^{0.45} \right] \tag{13}$$

$$f_{la} = \frac{E_f t_f}{R} \varepsilon_{h,rup} = \frac{2 E_f t_f}{D} \varepsilon_{h,rup} \tag{14}$$

where, t_f is the total thickness of the FRP jacket, $\varepsilon_{h,rup}$ is the rupture strain of FRP, E_f is the modulus of FRP, and D as shown in Eq. (15) is the diameter of equivalent circular column.

$$D = \sqrt{h^2 + b^2} \tag{15}$$

Shape factors:

$$k_{s1} = \left(\frac{b}{h} \right)^2 \frac{A_e}{A_c} \tag{16}$$

$$k_{s2} = \left(\frac{h}{b} \right)^{0.5} \frac{A_e}{A_c} \tag{17}$$

$$\frac{A_e}{A_c} = \frac{1 - \left((b/h)(h-2r)^2 + (h/b)(b-2r)^2 \right) / (3A_g) - \rho_s}{1 - \rho_s} \tag{18}$$

in which, b and h are the width and the depth of the cross section, r is the radius of the corner, ρ_s is the ratio of longitudinal steel reinforcement in the section.

3. Moment–rotation, hysteretic behaviour and inelastic analysis

3.1. Moment–curvature and moment–rotation curves

The models of concrete and steel are employed for the analysis of moment–curvature behaviour up to ultimate using the fibre model, in which the cross section is discretised into many fibres and the strain distribution is assumed to be linear while the stress in each fibre is based on the material models with the strain defined at the centroid of that fibre. The iterative loops of strain distribution stop when the equilibrium conditions are achieved. This procedure is continued until the curvature reaches its ultimate. This ultimate condition is considered to be the attainment of the ultimate strain in the concrete or longitudinal steel whichever comes first. In case of confinement by stirrups, the ultimate strain of concrete ε_{cm} and that of longitudinal steel ε_{sm}, as shown in Eqs. (19) and (20), respectively [30,31], are adopted. In case of FRP confinement, ε_{cm} is taken as ε_u shown in Eq. (13) in Lam and Teng [2,25] model, in which the rupture strain of the FRP $\varepsilon_{h,rup}$ is much smaller than its ultimate tensile strain ε_{frp}. Based on their experimental data, Lam and Teng [2] suggested $\varepsilon_{h,rup} = 0.624\varepsilon_{frp}$ for GFRP, which is used in this paper. It is worth mentioning that the ultimate strain of the longitudinal steel shown in Eq. (20) is also applied for the case of FRP confinement.

$$\varepsilon_{cm} = 0.004 + 1.4 \frac{\rho_s f_{yh} \varepsilon_{suh}}{f'_{cc}} \tag{19}$$

$$\varepsilon_{sm} = 0.6 \varepsilon_{su} \tag{20}$$

Fig. 2 shows typical moment–curvature curves of RC sections with and without FRP confinement. These curves include the cracking, yielding and ultimate points. The crack and yield points remain unchanged. The ultimate points are based on the lower of the two possible ultimates of the confined concrete and steel. The ultimate of unconfined concrete is also included for the sections without FRP. The moment–curvature curve after the ultimate is assumed to drop to 0. After the moment–curvature curves are obtained, simple plastic hinge model with the plastic hinge length $l_p = h$ proposed by Sheikh and Khoury [32] is used to compute moment–rotation curves, which are used for the properties of the nonlinear LINK elements.

3.2. Hysteretic behaviour of RC members

Hysteretic models for RC members available in the literature can be classified into two types: tri-linear and bi-linear hysteretic models. Tri-linear models include the cracking of concrete in the tension zone while the bilinear models exclude it. Amongst many available models, Takeda model [33] allows description of the damage of RC structures when the tension zone of concrete is cracked as shown in Fig. 3a, in which the coordinates (D_{cr}, P_{cr}) and (D_y, P_y) represent the cracking and yielding point, respectively; therefore, it is selected to be used in this paper. Seven rules were developed by Takeda et al. [33] to capture the response of the structures subjected to cyclic loads as briefly shown in Fig. 3b and c. The detail description of these rules can be found in Ref. [33].

3.3. Modelling technique for the inelastic time history analysis

Fig. 4 shows the theoretical background of the modelling for nonlinear analysis using the plastic hinge length technique. The beam with plastic hinge zone l_p in Fig. 4a corresponding to the idealised curvature in Fig. 4b is modelled by combining three types of elements: elastic, infinitely stiff and zero-length nonlinear LINK elements, which are illustrated in Fig. 4c. The nonlinear LINK element allows for the incorporation of the moment–rotation property of the plastic hinge, which behaves in accordance with the Takeda hysteretic model [33] described in Section 3.2. Therefore, the infinitely stiff elements can purely function as the connection.

Stiffness is another important issue to be taken into account for the elastic elements. ACI [34] uses the secant stiffness corresponding to yield point as the elastic stiffness; consequently, the modification factors for EI_g of beams and columns can be taken as 0.35 and 0.7, respectively. However, the original stiffness should be used in case the structures work in the pre-cracking range. To simplify, an approximation is made in this study: the infinitely stiff

Table 1
Damage levels.

Legend	Damage index	Description
.	>0–0.05	No or minor
+	0.05–0.25	Light
x	0.25–0.50	Moderate
▲	0.50–0.75	Severe
●	0.75–1.00	Collapse

Fig. 6. Three storey frame [48].

elements are replaced by the elastic elements shown in Fig. 4c. This is due to: (1) the elastic deformation of the assumed elastic elements with the length l_p seems to be minor, and (2) the modified stiffness may result in underestimated deformations when structures work in the plastic range beyond yield. This approximation provides some additional deformation from the assumed elastic elements which may compensate for the underestimation. As a result, the lumped plasticity model shown in Fig. 4d is used in this study and the nonlinear LINK locations of beams and columns in frames is shown in Fig. 5.

4. Damage models

Damage models available can be classified into two categories: non-cumulative and cumulative. Using cumulative damage models

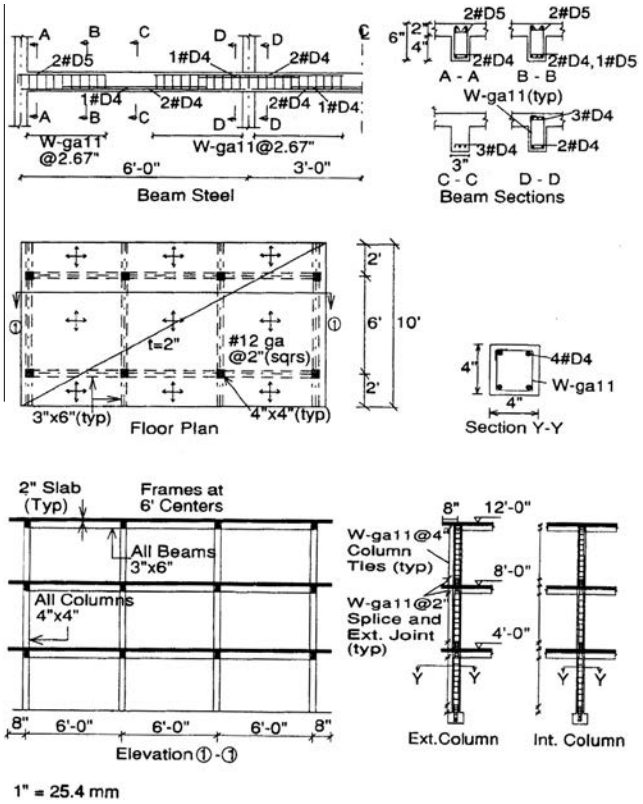

Fig. 7. Dimensions and reinforcement arrangement of three storey frame [48].

Table 2
Properties of reinforcement.

Reinforcement	Diameter (mm)	Yield strength (MPa)	Ultimate strength (MPa)	Modulus (MPa)	Ultimate strain
D4	5.715	468.86	503.34	214089.8	0.15
D5	6.401	262.01	372.33	214089.8	0.15
12 ga.	2.770	399.91	441.28	206160.5	0.13
11 ga.	3.048	386.12	482.65	205471	0.13

Table 3
Axial load in columns.

Storey	Axial load (kN)	
	External column	Internal column
1	30	60
2	20	40
3	10	20

is a more rational choice to evaluate damage states of structures subjected to earthquakes; hence, they are discussed here. Banon and Veneziano [35] simply used the normalised cumulative rotation as a damage index (*DI*), which is expressed by the ratio of the sum of inelastic rotations during half cycles to the yield rotation. A few years later, Park and Ang [36] proposed a *DI* incorporating both deformation and hysteretic energy as shown in Eq. (21), where, u_m is the maximum displacement of a single-degree-of-freedom (SDOF) system subjected to earthquake, u_u is the ultimate displacement under monotonic loading, E_h is the hysteretic energy dissipated by the SDOF system, F_y is the yield force and β is a parameter to include the effect of cyclic loading.

$$DI = \frac{u_m}{u_u} + \beta \frac{E_h}{F_y u_u} \tag{21}$$

Park and Ang [36] classified damage states into the following five levels:

$DI < 0.1$: No damage or localised minor cracking.
$0.1 \leqslant DI < 0.25$: Minor damage: light cracking throughout.
$0.25 \leqslant DI < 0.40$: Moderate damage: severe cracking, localised spalling.
$0.4 \leqslant DI < 1.00$: Severe damage: concrete crushing, reinforcement exposed.
$DI \geqslant 1.00$: Collapse.

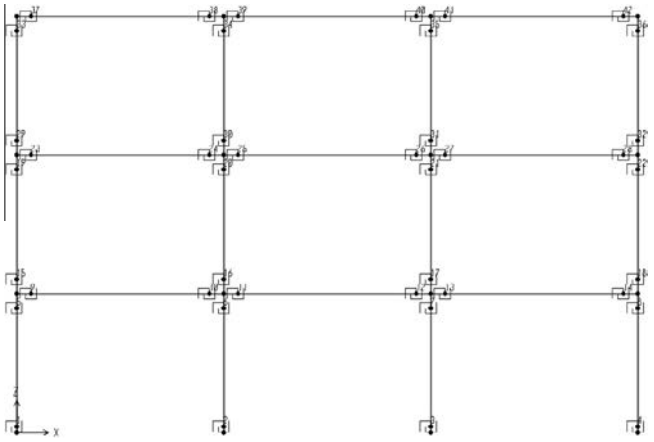

Fig. 8. Modelling of the three-storey frame with nonlinear LINK elements.

Table 4
Modal frequencies (Hz).

Mode	Experiment [48]	Model
1	1.78	1.70
2	5.32	5.30
3	7.89	9.03

$DI \geqslant 0.8$ has been suggested to represent collapse [37]. Park and Ang [36] also proposed *DI* for an individual storey and for an overall structure using the weighting factor based on the amount of hysteretic energy (E_i) absorbed by the element or the component.

Park and Ang [36] is the best known and the most widely used *DI* [38], largely due to its general applicability and the clear definition of different damage states provided in terms of *DI*. However, the following limitations are worth noting: $DI > 0$ when a structure works within elastic range and $DI > 1$ when the structure collapses with no specified upper limit for *DI*. Due to these limitations, Park and Ang's [36] concept has been modified by researchers such as Fardis et al. [39], Ghobarah and Aly [40], and Bozorgnia and Bertero [41]. However, the most significant modification was made by Kunnath et al. [42] who used the moment–rotation behaviour to replace the deformation terms used by Park and Ang [36] and subtracted the recoverable rotation as shown in Eq. (22), where, θ_m is the maximum rotation in loading history, θ_u is the ultimate rotation capacity, θ_r is the recoverable rotation when unloading and M_y is the yield moment. The merit of this modification is that *DI* will be 0 when structures work within elastic range. The major limitation to this proposal is, however, that the $DI > 1$ when the structure fails.

$$DI = \frac{\theta_m - \theta_r}{\theta_u - \theta_r} + \beta \frac{E_h}{M_y \theta_u} \tag{22}$$

The amount of energy absorbed by a structure is closely related to its corresponding damage state. Hence, *DI* may be expressed as the ratio of the hysteretic energy demand E_h to the absorbed energy capacity of a structure under monotonic loading $E_{h,u}$ [43–45]. However, this proposed *DI* has no specific upper limit to define the state of collapse.

In recognition of the energy parameter, which takes into account a number of parameters such as force, deformation and the number of cycles, Cao et al. [46] proposed a model which was later modified by the authors as shown in Eqs. (23)–(25).

$$DI = \left[\frac{E_h}{E_h + E_{rec}}\right]^{\alpha(N-i)} \tag{23}$$

$$N = \frac{E_{h,1collapse}}{E_{h,1y}} \tag{24}$$

$$i = \frac{E_h}{E_{h,1y}} \tag{25}$$

where $E_{h,1collapse}$ and $E_{h,1y}$ are the hysteretic energy of one complete ultimate and yielding cycle, respectively. Eqs. (24) and (25) define the proposed parameters *N* and *i*. *N* is the equivalent number of yielding cycles to collapse whilst *i* is the equivalent number of yielding cycles at the current time of loading ($i \leqslant N$). α is a modification factor and is proposed as 0.06 and the damage levels are shown in Table 1, in which the legends in the first column corresponding to the damage levels are used to express the damage in the studied cases presented in Sections 5 and 7.

5. Verification of the modelling technique

In order to validate the modelling technique mentioned above, a tested three-storey frame [47] is selected. Its details, and inelastic time history and damage analyses of the frame are described as follows.

5.1. Description of a tested three-storey frame [47]

The frame shown in Fig. 6 is a one-third scale three-storey RC frame designed only for gravity loads. Its dimensions and reinforcing details are presented in Fig. 7. Concrete strength varied from 20.2 to 34.2 MPa (the average can be taken as $f'_c = 27.2$ MPa), and the average modulus of elasticity was taken as $E_c = 24200$ MPa. Four types of reinforcement were used, and their properties are shown Table 2.

The Dead Loads were calculated from the self-weight of beams, columns, slabs and additional weights attached to the frame, as shown in Fig. 6. The total weight of each floor was found to be approximately 120 kN. Further details of this frame can be found in [47,48]. The seismic record selected for simulation was the N21E ground acceleration component of Taft earthquake occurred on 21 July 1952 at the Lincoln School Tunnel site in California. The peak ground accelerations (PGA) are 0.05 g, 0.20 g and 0.30 g representing minor, moderate and severe shaking, respectively.

5.2. Modelling and verification

The axial loads in columns are assumed to be constant during excitations and are shown in Table 3. Moment–rotations for all beams and columns were computed as described in Section 3.1. Axial loads on columns were taken into account; however, the effect of confinement was ignored due to relatively large stirrup spacing. Fig. 8 shows the model with nonlinear LINK elements in SAP2000. The hysteretic behaviour of these nonlinear elements follow the Takeda model [33]. The structural frequencies of the first three mode shapes are determined in Table 4 in comparison with the experimental results. They are very close in the first and second modes, but there is little difference in the third mode. However, the first mode plays the most important role.

Table 5
Comparison between experimental [48] and analytical results.

PGA	Storey	Maximum inter-storey drift (%)		Maximum storey displacement (mm)	
		Experiment	Model	Experiment	Model
0.05 g	3	0.23	0.21	7.6	7.9
	2	0.24	0.25	5.6	5.6
	1	0.28	0.23	3.6	2.8
0.20 g	3	0.54	0.83	33.5	38.9
	2	1.07	1.17	29.0	30.7
	1	1.33	1.31	16.3	16.0
0.3 g	3	0.89	1.18	59.7	58.4
	2	2.24	1.91	52.1	46.1
	1	2.03	1.96	24.6	23.9

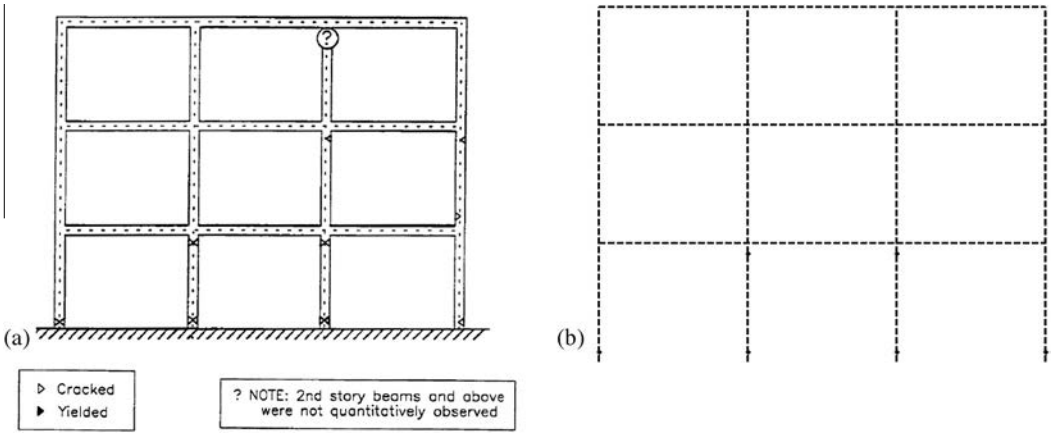

Fig. 9. Damage states – Taft 0.05 g: (a) Experiment [47]; (b) Analysis.

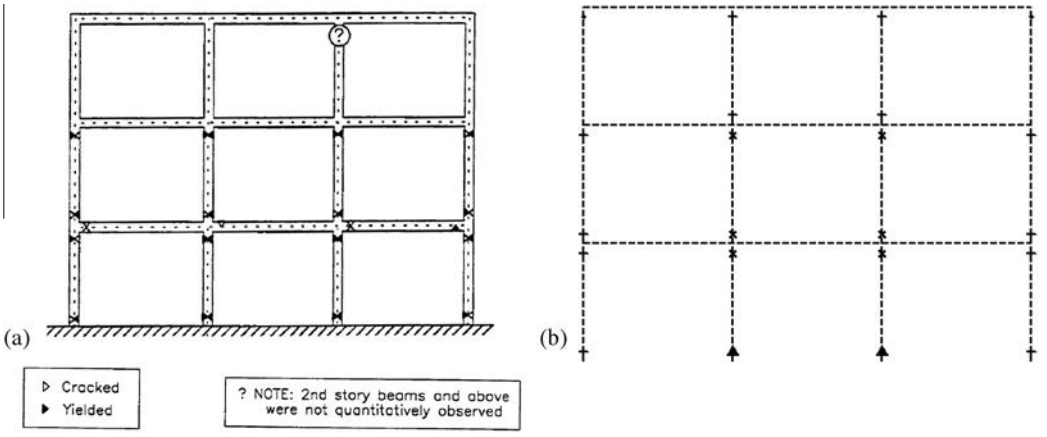

Fig. 10. Damage states – Taft 0.20 g: (a) Experiment [47]; (b) Analysis.

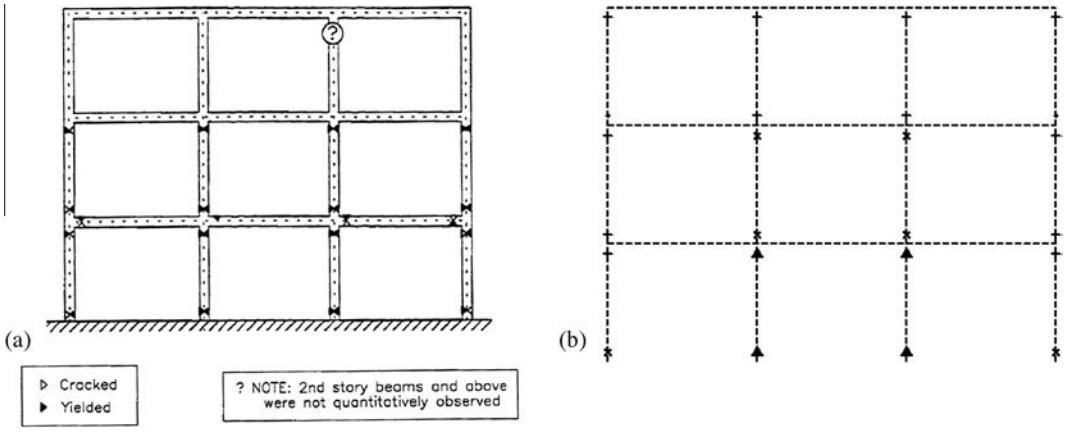

Fig. 11. Damage states – Taft 0.30 g: (a) Experiment [47]; (b) Analysis.

Inelastic time history analyses of the SAP2000 model subjected to the Taft earthquake ground motions are performed. The results in terms of maximum inter-storey drift and maximum storey displacement are presented in Table 5 in comparison with those obtained from experiment [48]. Though not an exact match, the model provides an overall good approximation.

5.3. Damage analyses and comparison

The selected damage model is employed to identify, locate and quantify the damage imparted to the structure during the excitation. Figs. 9–11a present the experimental damage states taken from [47] while Figs. 9–11b show the analytical damage states

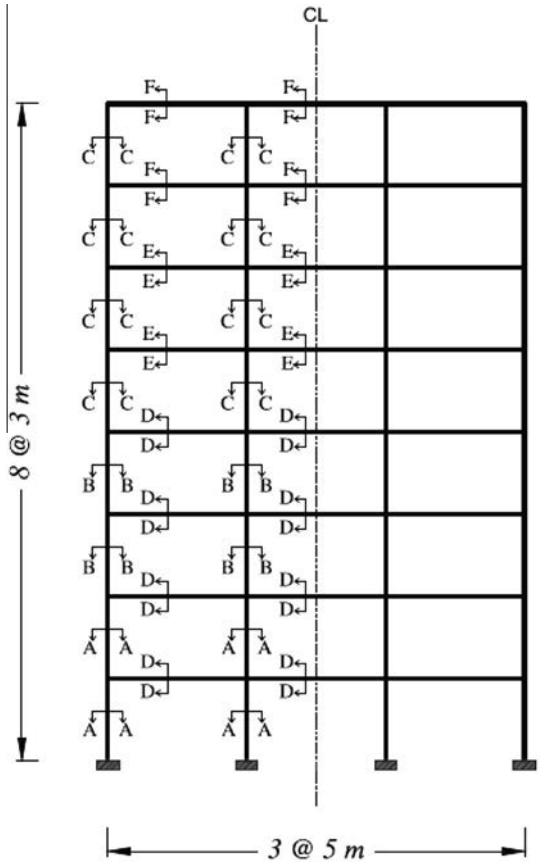

Fig. 12. Eight-storey frame [15,49].

for the Taft PGAs of 0.05 g, 0.20 g and 0.30 g, respectively. It should be noted that the analytical damage states are plotted for different damage index levels as described in Table 1. The damage states obtained from analyses are close to those obtained from experiment.

6. Eight-storey frames

6.1. Description of eight-storey frames

An 8-storey RC frame [15,49] shown in Fig. 12 with its typical column and beam sections shown in Fig. 13 is revisited. Its dimensions in millimetres and reinforcing details are shown in Table 6 with different shear steel spacing for intermediate and poorly-confined frames. Grade 60 (f_y = 420 MPa) steel and the concrete compressive strength of 25 MPa were used. The deformed steel bars of Φ10 mm were used for transverse reinforcement.

The design Live Load was 10 kN/m and the Dead Load was 30 kN/m in addition to the self-weight of the structure. The design seismic load was determined based on UBC 1994 [50]. The design

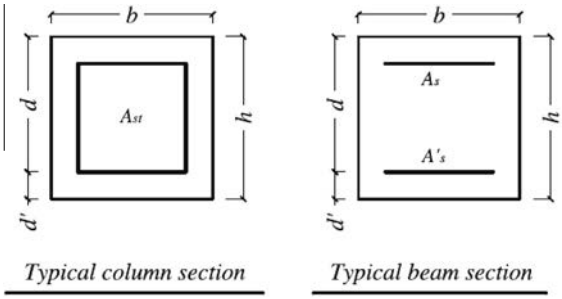

Fig. 13. Typical column and beam sections [15,49].

acceleration of 0.3 g representing for a high level of seismic hazard, and soil profile type III which is similar to class D in FEMA 356 [51] was used for the calculation of the design base shear. The corresponding design response spectrum divided by PGA is established as shown in Fig. 14.

6.2. Modelling and verification

The total Dead Load and 25% Live Load as recommended by many seismic codes are used for the inelastic time history analyses. The 8-storey frame is modelled using the modelling technique with SAP2000 nonlinear LINK elements described in Section 3.3. The properties of nonlinear LINK elements were determined based on moment–curvature and moment–rotation analyses presented in Section 3.1. The elastic modulus of concrete was taken as $E_c = 4700\sqrt{f'_c}$ [34], in which f'_c is the compressive strength of concrete. It is worth noting that the confinement effect is taken into account in this study case. The moment–curvature curves for columns and beams are computed using the average axial loads on them during an earthquake, which are corresponding to the axial loads determined from the static load case. The fundamental period (T) of the structure corresponding the full Dead Load and 25% Live Load is determined as 1.24 s which is close to the period 1.28 s modelled by Ronagh and Eslami [49].

6.3. Validation of the model using pushover analysis

The vertical distribution of the equivalent horizontal static seismic loads are computed in accordance with the Eq. (26) [50]. An additional force F_t as shown in Eq. (27) is applied for the top storey.

$$F_i = (V - F_t)\frac{W_i h_i}{\sum W_i h_i} \tag{26}$$

$$F_t = 0.07TV \leqslant 0.25V \tag{27}$$

in which, F_i is the lateral force at storey i, W_i is the seismic weight of storey i, which includes the Dead Load and 25% Live Load, h_i is the height of storey i, F_t is the additional force on the top storey, V is the shear force.

Table 6
Reinforcement details of the 8-storey intermediate and poorly-confined frames [15].

Section	b	h	d	d'	A_{st}	A_s	A'_s	Shear steel spacing	
								Intermediate	Poorly-confined
A–A	600	600	540	60	16Φ25	–	–	150	450
B–B	600	600	540	60	16Φ18	–	–	150	450
C–C	500	500	440	60	16Φ16	–	–	125	450
D–D	500	500	440	60	–	6Φ25	4Φ25	100	140
E–E	500	500	440	60	–	6Φ22	4Φ22	100	175
F–F	500	500	440	60	–	6Φ18	3Φ18	100	250

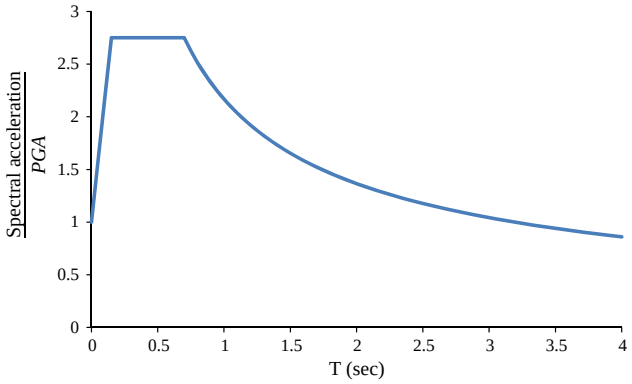

Fig. 14. Spectral acceleration/PGA.

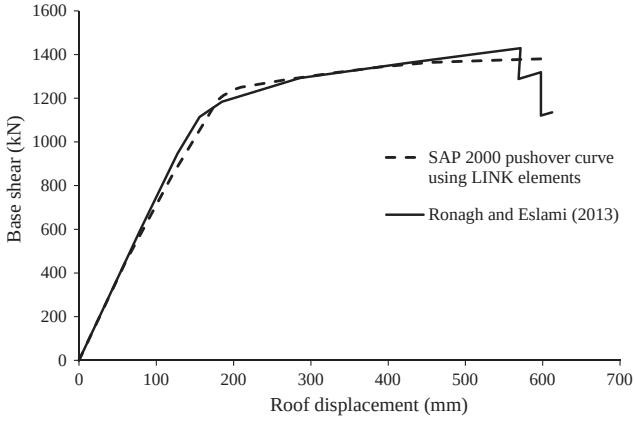

Fig. 15. Comparison of pushover curves.

The above lateral loads are applied to the model with SAP2000 nonlinear LINK elements and nonlinear static (pushover) analysis is performed. The obtained pushover curve is plotted in comparison with that performed by Ronagh and Eslami [49] as shown in Fig. 15. It shows a good overall approximation.

6.4. Selection of seismic records

The intensities equal or larger than the design PGA of 0.3 g are selected for damage analyses. They are selected as 0.3 g, 0.45 g and 0.6 g which are used to establish the corresponding spectra. These spectra are used as the target for scaling ground motions. The scaling criterion is based on ASCE [52] which requires that the mean value of the 5%-damped response spectra for the set of scaled ground motions is not less than the target response spectrum over the range of periods from $0.2T$ to $1.5T$, where $T = 1.24$ s is the fundamental period of the structure. In addition, the demand parameter such as drift, force and deformation can be calculated in different ways, depending on the number of ground motions in each set. If each set contains 7 ground motions or more, the demand parameter is the average value; otherwise, the maximum can be used for the demand parameter.

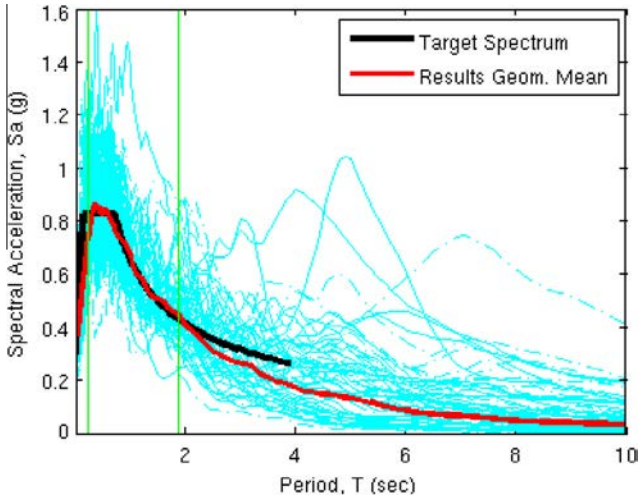

Fig. 16. Scaling records to match the target spectrum.

In this paper, ground motions used in this study are selected using the Pacific Earthquake Engineering Research Centre database software [53]. The selected records are scaled to match the target spectrum in a range of periods from $0.2T = 0.248$ s to $1.5T = 1.86$ s. Fig. 16 is an example of scaling results. Three sets of records with different intensities representing by PGAs 0.3 g, 0.45 g and 0.6 g are used. The effect of near-fault ground motions was not considered for the design; hence, pulse-type motions are not selected. Each set includes 14 scaled fault-normal and fault-parallel ground motion records of seven stations; therefore, the average value of the demand parameter is used. Table 7 shows the earthquake records with different Next Generation Attenuation number (NGA#) and scaling factors for three intensities obtained from the Pacific Earthquake Engineering Research Centre database software [53].

6.5. Designing and modelling of the retrofitted frame

Due to its much lower modulus which results in higher displacement ductility, and its comparatively lower cost in comparison to CFRP, GFRP is a better choice for the confinement purpose; therefore, it is selected in this paper. Table 8 shows the properties of GFRP materials provided by the manufacturer.

As stated, the objective of this study is to investigate the FRP confinement effect on the potential damage of RC structures subjected to earthquakes, the GFRP retrofitting design is presented in Fig. 17. The columns are rounded at the corners with a radius

Table 7
Ordinary records with scaling factors for the seismic intensities of 0.3 g, 0.45 g and 0.6 g.

No.	NGA#	Scale factor for intensity of			Event	Year	Station	Magnitude
		0.3 g	0.45 g	0.6 g				
1	1497	2.8719	4.3074	5.7432	Chi-Chi, Taiwan	1999	TCU057	7.62
2	1215	5.5179	8.2761	11.035	Chi-Chi, Taiwan	1999	CHY058	7.62
3	1488	3.1241	4.6857	6.2476	Chi-Chi, Taiwan	1999	TCU048	7.62
4	3441	32.4018	48.5983	64.798	Chi-Chi, Taiwan-06	1999	TCU007	6.3
5	2822	31.6713	47.5026	63.337	Chi-Chi, Taiwan-04	1999	KAU055	6.2
6	3537	15.0175	22.5242	30.032	Chi-Chi, Taiwan-06	1999	TTN032	6.3
7	1243	4.9909	7.4857	9.9809	Chi-Chi, Taiwan	1999	CHY100	7.62

Table 8
Properties of GFRP [54].

Tensile strength, f_{fr} (MPa)	Tensile modulus, E_f (MPa)	Thickness, t_f (mm)
3241	72379	0.589

of 50 mm and then wrapped by two layers of GFRP to provide external confinement. With the rounded corners, the GFRP confinement becomes more effective comparing to without rounding [55].

It is worth noting that the plastic hinge location is not affected by the GFRP confinement as evident in the columns retrofitted by GFRP wrap [7]. Hence, the locations of plastic hinges in the retrofitted frame are similar to those of the original frame. At the presence of GFRP confinement, the yield stiffness remains unchanged as the longitudinal reinforcement has not changed. This is also evident from the authors' analytical results shown in Fig. 2; therefore, the stiffness of the elastic column elements is unchanged. The properties of nonlinear LINK elements of beams are also unchanged as FRP is not applied to beams; however, these of columns are changed.

7. Results and discussions

Inelastic time history analyses are performed for the poorly-confined, intermediate frames and the FRP retrofitted frame subjected to the scaled ground motions corresponding to seismic intensities of 0.3 g, 0.45 g and 0.6 g as selected in Section 6.4. The results from inelastic time history analyses are used to conduct damage analyses and damage indices are obtained for all nonlinear LINK elements in accordance with 14 ground motions of each seismic intensity. Then, for every LINK element, the average damage

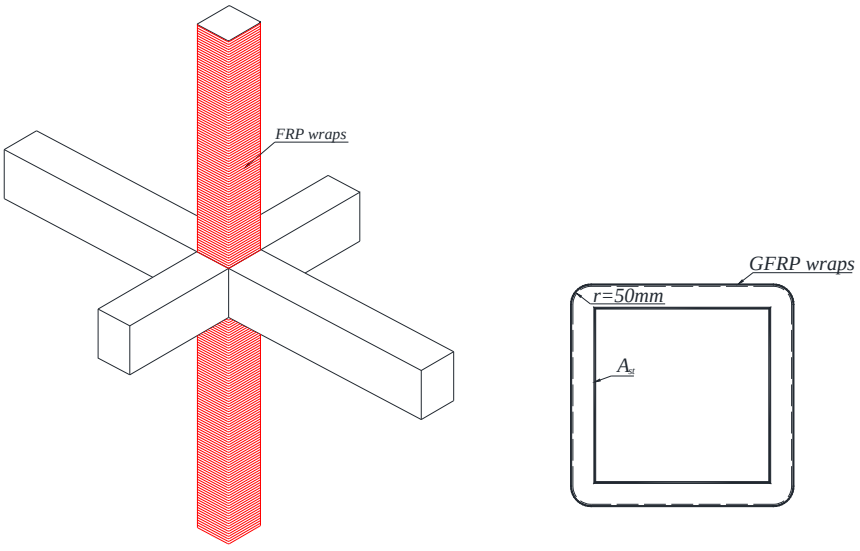

(a) GFRP wraps of columns

(b) A cross section of columns retrofitted by GFRP wraps

Fig. 17. Design of GFRP wrap to confine concrete.

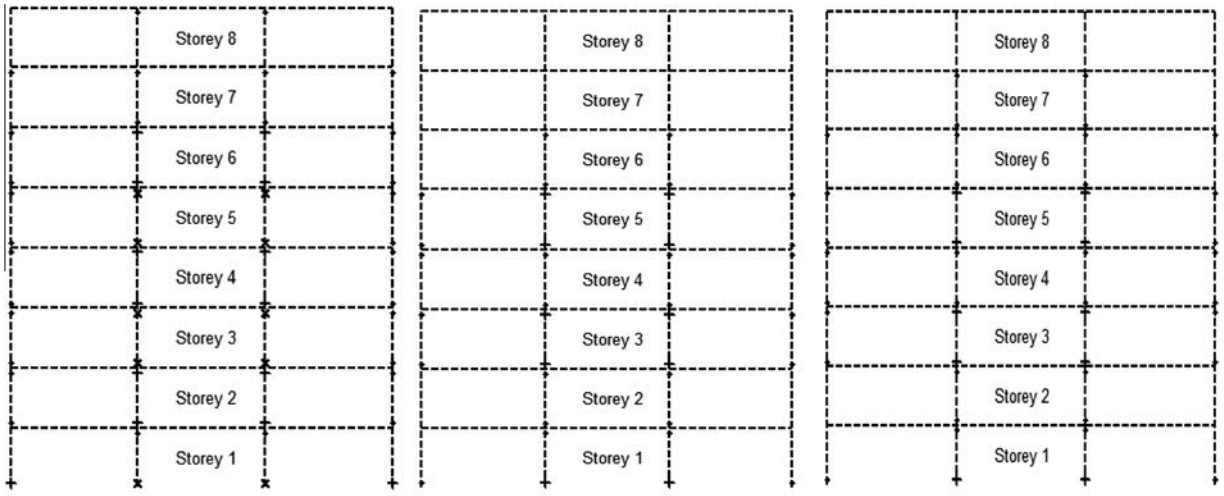

(a) Poorly-confined frame (b) Intermediate frame (c) Retrofit of the poorly-confined frame

Fig. 18. Damage modes of the 8-storey frames subjected to seismic intensity 0.3 g.

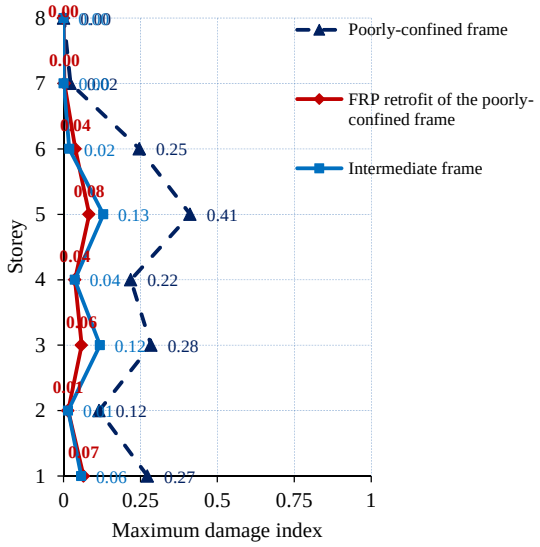

Fig. 19. Distribution of maximum damage indices of the 8-storey frames subjected to seismic intensity 0.3 g.

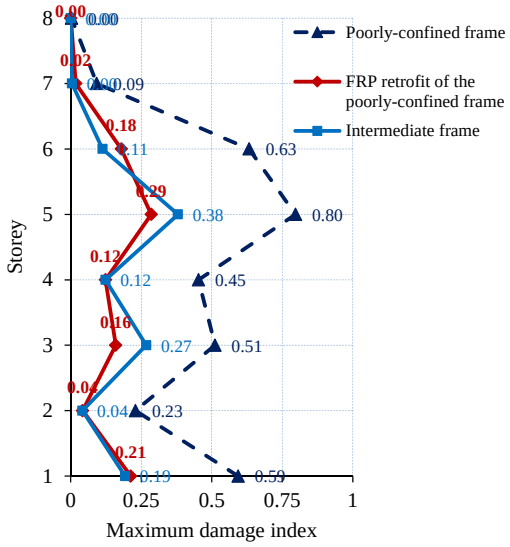

Fig. 21. Distribution of maximum damage indices of the 8-storey frames subjected to seismic intensity 0.45 g.

index (from 14 damage indices) corresponding to a seismic intensity is computed. The distribution of damage indices around the frames are plotted in Figs. 18, 20 and 22. It should be noted that the damage levels presented in these figures are provided in Table 1. The maximum damage indices in each storey are determined and plotted in Figs. 19, 21 and 23.

Figs. 18–23 show the damage in terms of damage index of the poorly-confined and FRP retrofitted frames in comparison to the intermediate frame when subjected to different seismic intensities. As is seen, the storey 5 suffers the most severe damage while the top storey experiences the least damage. Also, the damage in the two inner columns is more severe than that in the outer columns of the same storey. More damage in storey 1 comparing to storey 2 is due to higher axial forces and moments on the columns of the first storey. Noticeably, the damage of FRP retrofitted frame is significantly less than that of the original poorly-confined frame and is almost similar to or less than that of the intermediate frame.

For the seismic intensity of 0.3 g, the poorly-confined frame suffers moderate damage while the retrofitted frame experiences light damage which is similar to the damage state of the intermediate frame. There is no damage in beams of these frames. For the seismic intensity of 0.45 g, the storey 5 of the poorly-confined frame reaches the collapse state while the retrofitted frame experiences moderate damage that is similar to the damage of the intermediate frame. There is no or minor damage in beams of the poorly-confined and the retrofitted frames; though some minor damage is developed in beams of the intermediate frame. The FRP confinement effect brings the state of the poorly-confined frame down two damage levels from collapse to moderate. For the seismic intensity of 0.6 g, the poorly-confined frame collapses while the retrofitted frame suffers a severe damage state which is almost the same as the damage state of the intermediate frame. Generally, due to the FRP confinement effect, the damage state of the retrofitted frame is reduced one or two damage levels comparing to that

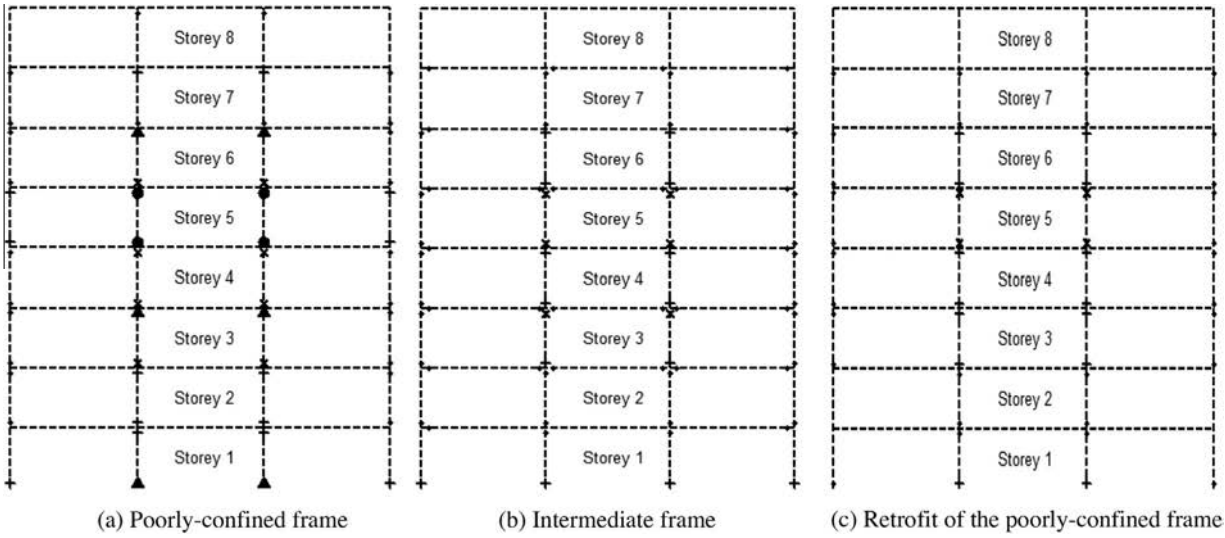

Fig. 20. Damage modes of the 8-storey frames subjected to seismic intensity 0.45 g.

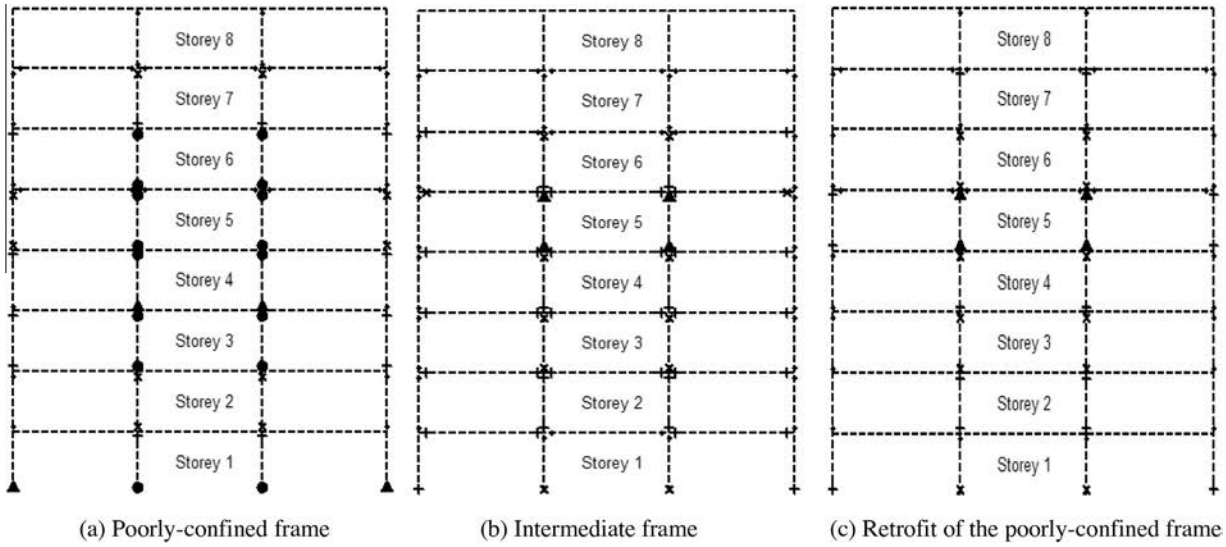

Fig. 22. Damage modes of the 8-storey frames subjected to seismic intensity 0.6 g.

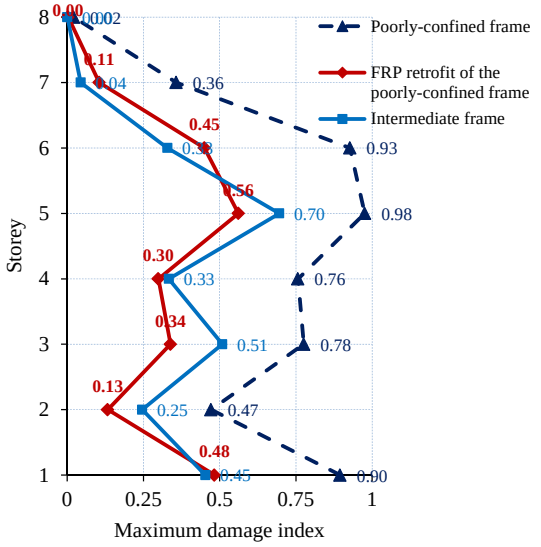

Fig. 23. Distribution of maximum damage indices of the 8-storey frames subjected to seismic intensity 0.60 g.

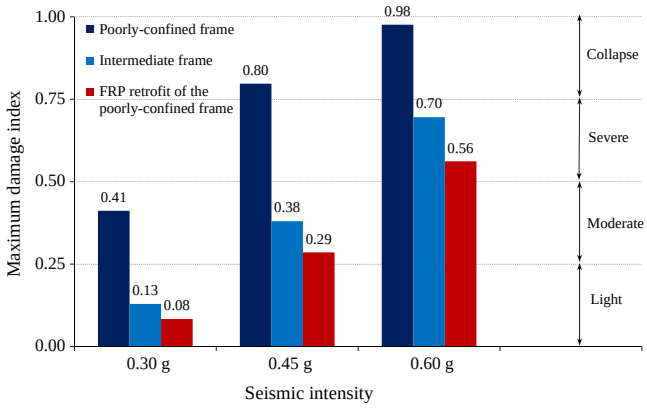

Fig. 24. Maximum damage indices of the poorly-confined, intermediate and the FRP retrofit of the poorly-confined frame.

Table 9
Reduction of damage indices.

Seismic intensity	$\text{Max}DI_{\text{original}} - \text{Max}DI_{\text{retrofitted}}$
0.30 g	0.33
0.45 g	0.51
0.60 g	0.42

of the poorly-confined frame; also the retrofitted frame suffers less damage in comparison to the intermediate frame as can be seen from Fig. 24.

The reduction of damage indices of the retrofitted frame is significant as shown in Fig. 24 and Table 9. The damage index of the retrofitted frame reduces by 0.33, 0.51 and 0.42 compared to that of the original poorly-confined frame when subjected to the seismic intensities of 0.30 g, 0.45 g and 0.60 g, respectively. This leads to significantly positive changes on damage states and demonstrates the effectiveness of the FRP confinement retrofit of the poorly-confined RC frames.

8. Conclusions

Inelastic time history and damage analyses of an 8-storey frame designed for 3 different conditions as (1) poorly-confined, (2) seismically detailed to the "intermediate" and (3) retrofitted by FRP confinement were performed at different seismic intensities. The confinement effect of FRP on the damage of the poorly-confined frame was investigated with the reference to the "intermediate" frame. Although the poor confinement of the transverse reinforcement is neglected, the effect of FRP confinement is confirmed to significantly reduce the damage index of the retrofitted frame by 0.33, 0.51 and 0.42 in comparison to that of the original if subjected to the seismic intensities of 0.30 g, 0.45 g and 0.60 g, respectively. Consequently, the damage of the poorly-confined frame is brought down one or two damage levels. The retrofitted frame suffers less damage than the "intermediate" frame also confirms the significant effect of FRP confinement. These demonstrate the FRP external confinement as an appropriate retrofitting solution for RC structures poorly-confined by the internal transverse reinforcement. With this retrofitting solution, poorly-confined RC frames can be upgraded to seismically designed frames. This significant

effect of FRP confinement is worth taking into account when retrofitting RC frames with the deficiency of transverse reinforcement.

References

[1] Paultre P, Légeron F. Confinement reinforcement design for reinforced concrete columns. J Struct Eng 2008;134(5):738–49.
[2] Lam L, Teng JG. Design-oriented stress–strain model for FRP-confined concrete. Constr Build Mater 2003;17:471–89.
[3] Wei Y-Y, Wu Y-F. Unified stress–strain model of concrete for FRP-confined columns. Constr Build Mater 2012;26:381–92.
[4] Samaan M, Mirmiran A, Shahawy M. Model of concrete confined by fiber composites. J Struct Eng 1998;124(9):1025–31.
[5] Pellegrino C, Modena C. Analytical model for FRP confinement of concrete columns with and without internal steel reinforcement. J Compos Constr 2010;14(6):693–705.
[6] Harajli MH, Rteil AA. Effect of confinement using fiber-reinforced polymer or fiber-reinforced concrete on seismic performance of gravity load-designed columns. ACI Struct J 2004;101(1):47–56.
[7] Sheikh SA, Yau G. Seismic behavior of concrete columns confined with steel and fiber-reinforced polymers. ACI Struct J 2002;99(1):72–80.
[8] Rahai A, Akbarpour H. Experimental investigation on rectangular RC columns strengthened with CFRP composites under axial load and biaxial bending. Compos Struct 2014;108:538–46.
[9] Mukherjee A, Joshi M. FRPC reinforced concrete beam-column joints under cyclic excitation. Compos Struct 2005;70:185–99.
[10] Balsamo A, Colombo A, Manfredi G, Negro P, Prota A. Seismic behavior of a full-scale RC frame repaired using CFRP laminates. Eng Struct 2005;27:769–80.
[11] Ludovico MD, Prota A, Manfredi G, Cosenza E. Seismic strengthening of an under-designed RC structure with FRP. Earthquake Eng Struct Dynam 2008;37:141–62.
[12] Ludovico MD, Manfredi G, Mola E, Negro P, Prota A. Seismic behavior of a full-scale RC structure retrofitted using GFRP laminates. J Struct Eng 2008;134(5):810–21.
[13] Garcia R, Hajirasouliha I, Pilakoutas K. Seismic behaviour of deficient RC frames strengthened with CFRP composites. Eng Struct 2010;32:3075–85.
[14] Mortezaei A, Ronagh HR, Kheyroddin A. Seismic evaluation of FRP strengthened RC buildings subjected to near-fault ground motions having fling step. Compos Struct 2010;92:1200–11.
[15] Eslami A, Ronagh HR. Effect of FRP wrapping in seismic performance of RC buildings with and without special detailing – a case study. Compos B Eng 2013;45(1):1265–74.
[16] Computers and Structures Inc. SAP2000 Version 14.1.0; 2009.
[17] Chan WL. The ultimate strength and deformation of plastic hinges in reinforced concrete frameworks. Mag Concr Res 1955;7(21):121–32.
[18] Baker ALL, Amarakone AMN. Inelastic hyperstatic frames analysis. In: Proceedings of the international symposium on the flexural mechanics of reinforced concrete, ASCE-ACI; 1964. p. 85–142.
[19] Roy HEH, Sozen MA. Ductility of concrete. In: Proceedings of the international symposium on the flexural mechanics of reinforced concrete, ASCE-ACI; 1964. p. 213–24.
[20] Soliman MTM, Yu CW. The flexural stress–strain relationship of concrete confined by rectangular transverse reinforcement. Mag Concr Res 1967;19(61):223–38.
[21] Sargin M, Ghosh SK, Handa VK. Effects of lateral reinforcement upon the strength and deformation properties of concrete. Mag Concr Res 1971;23(75–76):99–110.
[22] Kent DC, Park R. Flexural members with confined concrete. J Struct Div 1971;97(7):1969–90.
[23] Park R, Paulay T. Reinforced concrete structures. New York – London – Sydney – Toronto: John Wiley & Sons; 1975. p. 769.
[24] Park R, Priestley MJN, Gill WD. Ductility of square-confined concrete columns. J Struct Div 1982;108:929–50.
[25] Lam L, Teng JG. Design-oriented stress–strain model for FRP-confined concrete in rectangular columns. J Reinf Plast Compos 2003;22(13):1149–86.
[26] Harajli MH, Hantouche E, Soudki K. Stress–strain model for fiber-reinforced polymer jacketed concrete columns. ACI Struct J. September–October 2006;103(5):672–82.
[27] Wu G, Wu ZS, Lü ZT. Design-oriented stress–strain model for concrete prisms confined with FRP composites. Constr Build Mater 2007;21(5):1107–21.
[28] Youssef MN, Feng MQ, Mosallam AS. Stress–strain model for concrete confined by FRP composites. Compos B Eng 2007;38(5–6):614–28.
[29] Rocca S, Galati N, Nanni A. Interaction diagram methodology for design of FRP-confined reinforced concrete columns. Constr Build Mater 2009;23(4):1508–20.
[30] Paulay T, Priestley MJN. Seismic design of reinforced concrete and masonry buildings. New York – Chichester – Brisbane – Toronto – Singapore: Springer; 1992.
[31] Priestley MJN. Performance based seismic design. In: 12th world conference on earthquake engineering; 2000.
[32] Sheikh SA, Khoury SS. Confined concrete columns with stubs. ACI Struct J 1993;90(4):414–31.
[33] Takeda T, Sozen MA, Nielsen NN. Reinforced concrete response to simulated earthquakes. J Struct Div 1970;96:2557–73.
[34] ACI. Building code requirements for structural concrete (ACI 318M–08) and commentary; 2008.
[35] Banon H, Veneziano D. Seismic safety of reinforced members and structures. Earthquake Eng Struct Dynam 1982;10(2):179–93.
[36] Park Y-J, Ang AH-S. Mechanistic seismic damage model for reinforced concrete. J Struct Eng 1985;111(4):722–39.
[37] Tabeshpour MR, Bakhshi A, Golafshani AA. Vulnerability and damage analyses of existing buildings. In: 13th World conference on earthquake engineering; 2004. Paper No. 1261.
[38] Kim T-H, Lee K-M, Chung Y-S, Shin HM. Seismic damage assessment of reinforced concrete bridge columns. Eng Struct 2005;27:576–92.
[39] Fardis MN, Economu SN, Antoniou AN, Komodromos PJ, Sfakianakis MG. Damage measures and failure criteria – part I, Contribution of university of Patras. Final report of cooperative research on the seismic response of reinforced concrete structures – 2nd Phase; 1993.
[40] Ghobarah A, Aly NM. Seismic reliability assessment of existing reinforced concrete buildings. J Earthquake Eng 1998;2(4):569–92.
[41] Bozorgnia Y, Bertero VV. Evaluation of damage potential of recorded earthquake ground motion. Seismol Res Lett 2001;72(2):233.
[42] Kunnath SK, Reinhorn AM, Lobo RF. IDARC version 3.0: a program for the inelastic damage analysis of reinforced concrete structures. Report no NCEER-92-0022, National Center for Earthquake Engineering Research, State University of New York at Buffalo; 1992.
[43] Fajfar P. Equivalent ductility factors, taking into account low-cycle fatigue. Earthquake Eng Struct Dynam 1992;21:837–48.
[44] Cosenza E, Manfredi G, Ramasco R. The use of damage functionals in earthquake engineering: a comparison between different methods. Earthquake Eng Struct Dynam 1993;22(10):855–68.
[45] Rodriguez ME, Padilla D. A damage index for the seismic analysis of reinforced concrete members. J Earthquake Eng 2009;13(3):364–83.
[46] Cao VV, Ronagh H, Ashraf M, Hassan B. A new damage index for reinforced concrete structures subjected to seismic loads. The first international postgraduate conference on engineering, designing and developing the built environment for sustainable wellbeing – eddBE20 11. Queensland, Australia: The Queensland University of Technology; 2011. p. 194–9 [27–29 April].
[47] Bracci JM. Experimental and analytical study of seismic damage and retrofit of lightly reinforced concrete structures in low seismicity zones. Buffalo: State University of New York; 1992.
[48] Bracci JM, Reinhorn AM, Mander JB. Seismic retrofit of reinforced concrete buildings designed for gravity loads: performance of structural system. ACI Struct J 1995;92(5).
[49] Ronagh HR, Eslami A. On flexural retrofitting of RC buildings using GFRP/CFRP – a comparative study. Compos B 2013;46:188–96.
[50] ICBO. Uniform building code. Whittier, California: International Conference of Building Officials; 1994.
[51] ASCE. Prestandard and commentary for the seismic rehabilitation of buildings. Prepared for Federal Emergency Management Agency, FEMA Publication No 356. Washington, D.C.: Federal Emergency Management Agency; 2000.
[52] ASCE. Minimum design loads for buildings and other structures. ASCE/SEI 7–10: American Society of Civil Engineers; 2010.
[53] PEER. PEER ground motion database. http://peer.berkeley.edu/peer_ground_motion_database. 2011.
[54] Luca AD, Nardone F, Matta F, Nanni A, Lignola GP, Prota A. Structural evaluation of full-scale FRP-confined reinforced concrete columns. J Compos Constr 2011;15(1):112–23.
[55] Wang L-M, Wu Y-F. Effect of corner radius on the performance of CFRP-confined square concrete columns: test. Eng Struct 2008;30:493–505.